Advances in Aircraft and Spacecraft Science, *Vol. 5, No. 6 (2018) 633-652*
DOI: https://doi.org/10.12989/aas.2018.5.6.633

Numerical simulation of the thermoelectric behavior of CNTs/CFRP aircraft composite laminates

Yueguo Lin[1a], Marie Christine Lafarie-Frenot[2], Jinbo Bai[3] and Marco Gigliotti*[2]

[1]*Department of Design and Manufacture of Aircrafts, Civil Aviation University of China, CAUC, 2898, Road Jinbei, District Dongli, 300300 Tianjin, China*
[2]*Institut Pprime, CNRS – ENSMA – Université de Poitiers, Département Physique et Mécanique de Matériaux, ENSMA – Téléport 2 – 1, Avenue Clément Ader, BP 40109, 86961 Futuroscope Chasseneuil Cedex, France*
[3]*CentraleSupélec, Université Paris-Saclay 3 rue Joliot-Curie, 91190 Gif-sur-Yvette, France*

(Received November 30, 2017, Revised March 20, 2018, Accepted March 21, 2018)

Abstract. The present paper focuses on the development of a model for simulating the thermoelectric behavior of CNTs/CFRP Organic Matrix Composite (OMC) laminates for aeronautical applications. The model is developed within the framework of the thermodynamics of irreversible processes and implemented into commercial ABAQUS Finite Element software and validated by comparison with experimental thermoelectric tests on two types of composites materials, namely Type A with Carbon Nanotubes (CNT) and Type B without CNT. A simplified model, neglecting heat conduction, is also developed for simplifying the identification process. The model is then applied for FEM numerical simulation of the thermoelectric response of aircraft panel structures subjected to electrical loads, in order to discuss the potential danger coming from electrical solicitations. The structural simulations are performed on quasi-isotropic stacking sequences (QI) $[45/-45/90/0]_s$ using composite materials of type A and type B and compared with those obtained on plates made of metallic material (aluminum). For both tested cases—transit of electric current of intermediate intensity (9A) and electrical loading on panels made of composite material—higher heating intensity is observed in composites materials with respect to the corresponding metallic ones.

Keywords: CNTs/CFRP laminates; thermoelectric behavior; numerical simulations, temperature field

1. Introduction

The use of CFRP Organic Matrix Composite (OMC) materials for fuselage structures can significantly reduce the weight of an aircraft, making CFRP materials widely employed in aircraft manufacturing.

However, aircraft fuselages may serve as "mass" and Faraday cages, therefore composite fuselage panels may be subjected to unwanted electric solicitations, such as for instance, electrical currents due to lightning strikes (high magnitude, kA, applied for a very short lapse of time, ns or μs), ordinary electrical currents due to the aircraft electronic devices (relatively low magnitude, few A, up to 10A and relatively high frequency, up to 1kHz), electrical currents due to the accumulation of static charges on the fuselage surfaces (relatively low magnitude, depending on the geometry and the arrangement of the panel-to-panel interfaces and gaps). These currents may

*Corresponding author, Professor, E-mail: marco.gigliotti@ensma.fr
[a] Ph.D., E-mail: yueguolin@yahoo.com

http://www.techno-press.org/?journal=aas&subpage=7 ISSN: 2287-528X (Print), 2287-5271 (Online)

Table 1 Type and dimensions of employed samples

sample n.	Type + Stacking sequences		Dimensions
#1	Type A (with CNTs)	$[0]_8$	L_x = 165mm, L_y = 18mm, e = 2mm
#2		$[0/90]_4$	
#3	Type B (without CNTs)	$[0]_8$	
#4		$[0/90]_4$	

promote Joule heating.

The study of the thermoelectric behavior of OMC for fuselage parts is therefore of paramount importance to understand the performance of such structures.

Some recent research work has been devoted to the study of the thermoelectric behavior of OMC (Gigliotti *et al.* 2011), highlighting the importance of current intensity and duration on Joule heating phenomena (Sierakowski *et al.* 2008), on mechanical static and fatigue performance (Gigliotti *et al.* 2015).

These works show that OMC are particularly sensitive to thermoelectric phenomena, this is mainly related to the scarce electrical conductive character of polymer matrices (Sierakowski *et al.* 2008, Gigliotti *et al.* 2011). Moreover electrical resistance of composite materials is particularly sensitive to damage (Xia *et al.* 2003), especially fiber breaks, since the electrical conductive paths along the composite are affected by such kind of damage.

In order to increase the thermoelectric performance of OMC, Carbon NanoTubes (CNT) have been employed in recent years, with promising results, since such materials have the potential to increase the thermal and electrical performance of polymer matrices (if dispersed in the matrix) and of the fiber-fiber electrical contacts (if attached to the fiber surfaces, Lin *et al.* 2015a, b), globally leading to an increase of the percolation behavior of the mixture. The thermoelectric behavior of CNT/CFRP materials can be significantly enhanced with respect to classical composite configurations (Lin *et al.* 2015a, b).

The current literature lacks of coupled models for the prediction of the thermoelectric response of OMC materials.

The present paper focuses on the development of a model for simulating the thermoelectric behavior of CNTs/CFRP Organic Matrix Composite (OMC) laminates for aeronautical applications. The model is developed within the framework of the thermodynamics of irreversible processes and implemented into commercial ABAQUS Finite Element software and validated by comparison with experimental thermoelectric tests on two types of composites materials, namely Type A with Carbon Nanotubes (CNT) and Type B without CNT. The model is then applied for FEM numerical simulation of the thermoelectric response of aircraft panel structures subjected to electrical loads, in order to discuss the potential danger coming from electrical solicitations. The structural simulations are performed on quasi-isotropic stacking sequences (QI) $[45/-45/90/0]_s$ using composite materials of type A and type B and compared with those obtained on plates made of metallic material (aluminum). For both tested cases, passage of electric current of intermediate intensity (9A), panels made of composite material shows a greater heating than the corresponding metallic ones.

During the thermoelectric test, dimensions and electrodes of sample are chosen in order to generate a homogeneous temperature field along the sample and to minimize the contact resistance; the electrical solicitations were selected carefully so that sample temperature would not exceed the glass transition temperature T_g of the resin, the contributions of Joule heat and contact

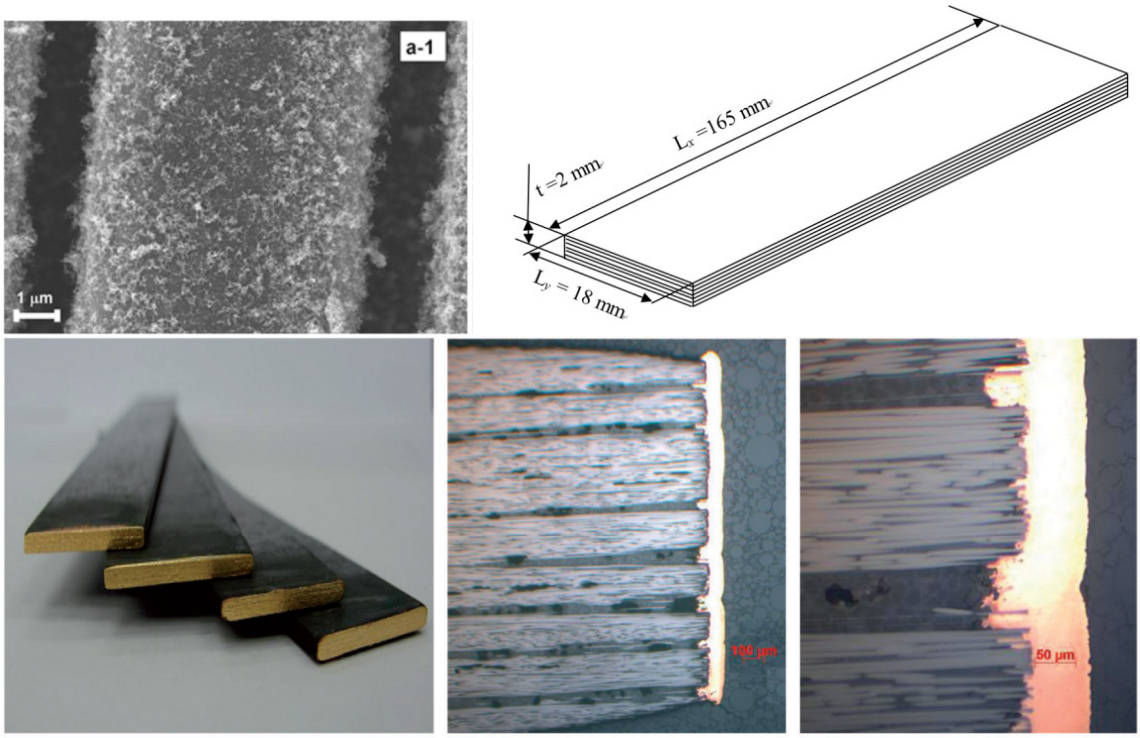

Fig. 1 CNTs/CFRP specimens with copper deposited electrodes and schematic sample geometry (taken from Lin *et al.* 2015a, b)

resistance heat are specifically presented in this paper. The finite element models were presented in detail to represent the thermoelectric tests data and then compared with the experiments results. All the apparatus which has been involved in the experiment and simulation process is described in detail in the paper.

2. Experimental materials and equipment

Materials. The composite used in this study is manufactured with the T700GC 12K carbon fibers as reinforcement and Epoxy M21 as matrix, currently used in aeronautical and aerospace industry. The geometry of the composite sample is 165mm × 18mm × 2mm and the average ply thickness is 0.25mm. Two types of stacking sequences are employed, namely unidirectional (UD) $[0]_8$ and cross orthogonal (CR) $[0/90]_4$, as shown in Table 1.

The volume fraction of carbon fibers in the composite material is around 56%. In order to increase the electrical conductivity and shear strength of the fiber-matrix interface, CNT are grown on the surface of carbon fibers through chemical vapor deposition (CVD) (Zhao *et al.* 2004, Saba *et al.* 2013).

Fig. 1 (taken from Lin *et al.* 2015a, b) shows the scanning electron microscope (SEM) images of CNT on the surface of carbon fiber (~2% wt of CNTs).

All samples are equipped with Prodec® surface electrodes realized by copper electrodepositing (around 50-60 μm thick) on the chemically polished surface edges of the samples.

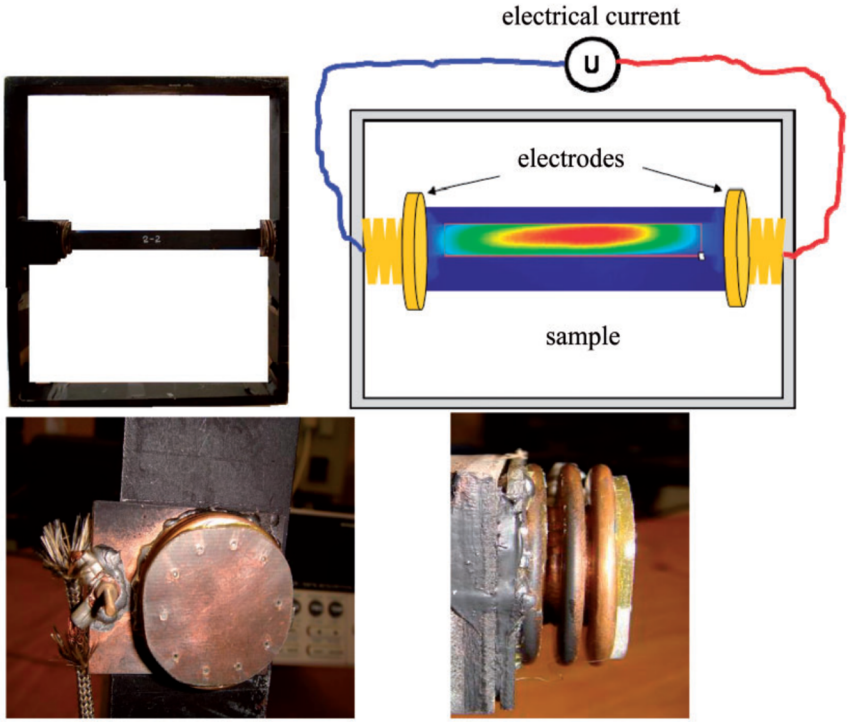

Fig. 2 Experimental setup for thermoelectric tests (Lin *et al.* 2015a, b)

Fig. 2 shows the experimental setup employed for thermoelectric test (Lin *et al.* 2015a, b): The sample can be placed either horizontally or vertically with both ends being in contact with a copper electrode, which is further connected with a mechanical spring in order to provide necessary contact pressure, so the CNTs/CFRP sample, the electrodes, a generator together with the electric wires form a close loop for the current flow. DC electric currents from 1A to 9A are injected by an electric generator, without inducing excessive local heating or exceeding the resin glass transition.

According to the preliminary thermoelectric tests (Gigliotti *et al.* 2011), the average induced temperature is around 60°C at 3A and around 160°C at 6A. The temperature is injected by steps of 1A and the temperature field is measured on the sample surface by a CEDIP 420M infrared thermography camera (Fig. 2b), with precision higher than 1°C and spatial resolution 320pixels × 256pixels, with a surface of 0.3mm × 0.3mm for each pixel. The experimental data are then post-processed using the Altair software, giving the temperature profiles and the voltage as function of time at each point of the exposed surface.

3. Modelling of the thermoelectric coupling

3.1 Development of the thermoelectric coupled model

The starting point of the model approach is the balance equation of a physical field (scalar, vector ...) k(**x**, t), depending mainly on the space and time; in local form this is given by (Muller 1973)

$$\frac{\partial k}{\partial t} + \nabla \cdot (k\mathbf{v}) + \nabla \cdot \mathbf{j}_{cond}[K] = \sigma[K], \tag{1}$$

where in

$$\nabla = \mathbf{i}\frac{\partial}{\partial x} + \mathbf{j}\frac{\partial}{\partial y} + \mathbf{k}\frac{\partial}{\partial z},$$

k(**x**, t) represents the mathematical density of a physic property K(t), depending only on the times, while σ[K] indicates the output (source) per unit time and unit volume and $\mathbf{j}_{cond}[K]$ is the conductive flux density. Muller (1973) introduces a distinction between intrinsic source $\sigma_v[K]$ and a source connected to remote source $\sigma_s[K]$. In general we propose that K(t) has the property of conservation:

$$\sigma_V[K] = 0 \tag{2}$$

Eq. 2 indicates that the intrinsic source is equal to zero.

Eq. 1 can be re-written as follows

$$\frac{\partial k}{\partial t} + \nabla \cdot \mathbf{j}_{cond}[K] = \sigma[K] \tag{3}$$

characterized by the presence of a total flow **j**[K], given by the sum of the conductive flow, $\mathbf{j}_{cond}[K]$ and a convective flow $\mathbf{j}_{conv}[K] = k\mathbf{v}$.

A second alternative form to Eq.1 is present as follows

$$\frac{dk}{dt} + \nabla \cdot \mathbf{j}_{cond}[K] = \sigma[K] \tag{4}$$

exploiting the concept of total derivative

$$\frac{d}{dt} = \frac{\partial}{\partial t} + \mathbf{v}\nabla \tag{5}$$

Before addressing the modeling of the thermoelectric coupling, we firstly consider the case of electrical conduction in the absence of thermal effects. In a rigid conductor, according to Eq. 6, the balance of electric charge per unit volume, ρz (z is the electric charge per unit mass), is expressed by

$$\rho\frac{dz}{dt} + \nabla \cdot \mathbf{i} = 0 \tag{6}$$

In this equation it is necessary to identify and explicit the term **i** and the flow conduction z (conduction current density): **i** is the electric current per unit area. It is noted that, in this case, the current source is zero; it is assumed that the electric current can not to be created (or destroyed) into a material element.

The balance of the internal energy equation (**E**) per unit volume, ρe, is written in the form

$$\rho\frac{de}{dt} = \mathbf{E} \cdot \mathbf{i} \tag{7}$$

where **E** is the electric field. In the absence of thermal effects, the internal energy flow is zero, its production (source) is represented by the term dissipative $\mathbf{E}\cdot\mathbf{i}$.

The entropy balance equation (S) per unit volume, ρs, can be written as

$$\rho\frac{ds}{dt}-\nabla\cdot\left(\frac{\mu_e}{z_e}\frac{\mathbf{i}}{T}\right)=\left(\mathbf{E}-\nabla\frac{\mu_e}{z_e}\right)\cdot\frac{\mathbf{i}}{T} \tag{8}$$

where μ_e is the chemical potential of the electrons and z_e is the mass fraction of the electrons. Comparing Eq. 4 with Eq. 8 the conductive flow of entropy can be easily identified

$$\mathbf{j}_{cond}[S]=-\frac{\mu_e}{z_e}\frac{\mathbf{i}}{T} \tag{9}$$

and the intrinsic entropy production is

$$\sigma[S]=\sigma_V[S]=\left(\mathbf{E}-\nabla\frac{\mu_e}{z_e}\right)\cdot\frac{\mathbf{i}}{T} \tag{10}$$

Eq.10 suggests, for a homogeneous and isotropic material, a linear relationship between flux and thermodynamic force

$$\left(\mathbf{E}-\nabla\frac{\mu_e}{e_e}\right)=\rho_e\mathbf{i} \tag{11}$$

where ρ_e is the electrical resistivity of the medium: Then, for negligible values of $\nabla\frac{\mu_e}{e_e}$, Eq. 11 takes the following form

$$\mathbf{E}=\rho_e\mathbf{i} \tag{12}$$

which represents the Ohm's law; using the Eq. 12 in Eq. 10 dissipation, the production of temperature and intrinsic entropy, takes the form

$$T\sigma[S]=T\sigma_V[S]=\rho_e i^2 \tag{13}$$

which represents the dissipation by Joule effect. In considering that in dissipative process dissipation must be always positive, Eq. 13 states that the resistivity of a medium is strictly positive. For a homogeneous and anisotropic material the scalar quantity ρ_e is replaced by a second order tensor (**ρ**, electrical resistivity tensor) which is assumed symmetrical (based on the postulate of Onsager (De Groot and Mazur 1969)) but not necessarily diagonal.

In the case of thermoelectric coupling the internal energy balance, Eq. 7, has to be enriched with a term taking into account the heat conduction. Then

$$\rho\frac{de}{dt}+\nabla\cdot\mathbf{q}=\mathbf{E}\cdot\mathbf{i} \tag{14}$$

in this case, shows that the internal power flow is given by the heat flow, **q**.

The new entropy balance—taking into account the exchange of thermal origin—becomes

$$\rho\frac{ds}{dt}+\nabla\cdot\left(\frac{\mathbf{q}}{T}-\frac{\mu_e}{z_e}\frac{\mathbf{i}}{T}\right)=\left(\mathbf{E}-\nabla\frac{\mu_e}{z_e}\right)\cdot\frac{\mathbf{i}}{T}-\frac{1}{T}\left(\frac{\mathbf{q}}{T}-\frac{\mu_e}{z_e}\frac{\mathbf{i}}{T}\right)\cdot\nabla T \tag{15}$$

in which the entropy flow takes the form

$$\mathbf{j}[S]=\frac{\mathbf{q}}{T}-\frac{\mu_e}{z_e}\frac{\mathbf{i}}{T} \tag{16}$$

and a source term (intrinsic) has the form

$$\sigma[S]=\sigma_V[S]=\left(\mathbf{E}-\nabla\frac{\mu_e}{z_e}\right)\cdot\frac{\mathbf{i}}{T}-\frac{1}{T}\left(\frac{\mathbf{q}}{T}-\frac{\mu_e}{z_e}\frac{\mathbf{i}}{T}\right)\cdot\nabla T \tag{17}$$

Following a standard procedure in the framework of thermodynamics of irreversible processes (De Groot and Mazur 1969), the evolution equations for entropy flow and electric current—for a homogeneous and isotropic medium—are respectively obtained using phenomenological expressions of the type

$$\mathbf{j}[S]=-L_{11}\nabla T+L_{12}\left(\mathbf{E}-\nabla\frac{\mu_e}{z_e}\right) \tag{18}$$

$$\mathbf{i}=-L_{21}\nabla T+L_{22}\left(\mathbf{E}-\nabla\frac{\mu_e}{z_e}\right) \tag{19}$$

where L_{11}, L_{12}, L_{21} and L_{22} are the phenomenological Onsager coefficients, with $L_{12} = L_{21}$, according to the Onsager-Casimir symmetry relationship (De Groot and Mazur 1969).

Eqs. 18-19 can be re-written as

$$\mathbf{q}=-\lambda\nabla T+\left(\pi+\frac{\mu_e}{z_e}\right)\mathbf{i} \tag{20}$$

$$\left(\mathbf{E}-\nabla\frac{\mu_e}{z_e}\right)=\varepsilon\nabla T+\rho_e\mathbf{i} \tag{21}$$

which introduce a new set of phenomenological coefficients

$$\lambda=T\left(L_{11}-\frac{L_{12}L_{21}}{L_{22}}\right) \tag{22}$$

$$\pi=T\frac{L_{12}}{L_{22}} \tag{23}$$

$$\varepsilon = \frac{L_{21}}{L_{22}} \tag{24}$$

$$\rho_e = \frac{1}{L_{22}} \tag{25}$$

a linear combination of Onsager coefficients which represent, respectively, the thermal conductivity (λ), the Peltier coefficient (π), the Seebeck coefficient (ε) and the electrical resistivity (ρ_e) of the medium. Note that—according to the Onsager-Casimir symmetry relations ($L_{12} = L_{21}$)—it follows that $\pi = T\varepsilon$.

Using Eqs. 14-17 and the phenomenological coefficients (Eqs. 22-25), the internal energy balance equation becomes

$$\rho \frac{de}{dt} = \nabla \cdot (\lambda \nabla T) + \rho_e i^2 - \mathbf{i} \cdot (\nabla \pi)_T + \left(\frac{\pi}{T} - \frac{\partial \pi}{\partial T} \right) \mathbf{i} \cdot \nabla T \tag{26}$$

where T indicates the temperature.

By defining the internal energy of the medium as the product of the specific capacity at constant volume, c_v and the temperature, the heat equation becomes

$$\rho \frac{dc_v T}{dt} = \nabla \cdot (\lambda \nabla T) + \rho_e i^2 - \mathbf{i} \cdot (\nabla \pi)_T + \left(\frac{\pi}{T} - \frac{\partial \pi}{\partial T} \right) \mathbf{i} \cdot \nabla T \tag{27}$$

which replacing the classical heat equation (Fourier equation) in the presence of thermoelectric coupling. According to Eq. 27, if the temperature is uniform only the Joule effect ($\rho_e i^2$ term) and the Peltier effect (term $\mathbf{i} \cdot (\nabla \pi)_T$) contribute to the heat dissipation. If temperature gradients occur, an additional term ($\left(\frac{\pi}{T} - \frac{\partial \pi}{\partial T} \right) \mathbf{i} \cdot \nabla T$)—normally indicated as «heat dissipation by Thompson effect»—comes into play.

For a homogeneous anisotropic material, Eq. 27 is still valid, but, in this case, the scalar coupling coefficients are replaced by tensors. For example, the thermal conductivity coefficient, λ, is replaced by the conductivity second order tensor, $\boldsymbol{\lambda}$, which in an orthonormal coordinate system (O, x, y, z) can be expressed by the square (3 × 3) matrix

$$\boldsymbol{\lambda} = \begin{bmatrix} \lambda_{xx} & \lambda_{xy} & \lambda_{xz} \\ \lambda_{yx} & \lambda_{yy} & \lambda_{yz} \\ \lambda_{zx} & \lambda_{zy} & \lambda_{zz} \end{bmatrix} \tag{28}$$

Similarly, the electrical resistivity of the medium, ρ_e, is replaced by the electric resistivity tensor, $\boldsymbol{\rho}$, the inverse of which, $\boldsymbol{\sigma}$, represents the electric conductivity tensor

$$\boldsymbol{\rho} = \begin{bmatrix} \rho_{xx} & \rho_{xy} & \rho_{xz} \\ \rho_{yx} & \rho_{yy} & \rho_{yz} \\ \rho_{zx} & \rho_{zy} & \rho_{zz} \end{bmatrix} \quad \text{and} \quad \boldsymbol{\sigma} = \begin{bmatrix} \sigma_{xx} & \sigma_{xy} & \sigma_{xz} \\ \sigma_{yx} & \sigma_{yy} & \sigma_{yz} \\ \sigma_{zx} & \sigma_{zy} & \sigma_{zz} \end{bmatrix} \tag{29}$$

If one accepts the Onsager-Casimir reciprocity postulate, these matrices become symmetrical; in a principal reference system, the matrices become also diagonal.

In particular, for an orthotropic composite material, in the orthotropic frame (O, L, T, E) matrices are in the form

$$\boldsymbol{\rho} = \begin{bmatrix} \rho_L & 0 & 0 \\ 0 & \rho_T & 0 \\ 0 & 0 & \rho_E \end{bmatrix} \quad \text{and} \quad \boldsymbol{\sigma} = \begin{bmatrix} \sigma_L & 0 & 0 \\ 0 & \sigma_T & 0 \\ 0 & 0 & \sigma_E \end{bmatrix} \tag{30}$$

The equations of the coupled thermoelectric model must be solved by using the proper boundary and initial conditions.

For the solution of the heat equation, Eq. 27, the temperature field and the heat flow must be specified on the external boundary (or part of it) of the material sample.

Two types of heat flow can be specified:

- heat flow by convection, q_c, expressed by a relation of the type

$$q_c = hA(T - T_a) \tag{31}$$

where h is the convection coefficient, T_a is the ambient temperature, A is the exchange surface with the environment,

- flow of heat by radiation, q_r, expressed by a relation of the type

$$q_r = \sigma\varepsilon(T^4 - T_a^4) \tag{32}$$

where σ and ε are a physical constant, respectively, the Stefan-Boltzmann constant ($\sigma = 5.67 \times 10^{-8}$ W/m^2K^4) and the emissivity of the surface, depending on the type of radiating surface.

The electric field and the electric current inside the material medium can be calculated by imposing the electric potential, φ, on a part of the boundary of the domain and using the relationship

$$\mathbf{i} = \boldsymbol{\sigma}\mathbf{E} = -\boldsymbol{\sigma}\nabla\varphi \tag{33}$$

3.2 Implementation within the ABAQUS FE Commercial Code

The implementation of the thermoelectric model in the finite element commercial code ABAQUS (Dassault Systemes Simulia Corp. 2009) can be done by using two different strategies:

- by employing the HEAT TRANSFER ABAQUS module: In this case the classical Fourier equation is solved by adding several potential heat sources (heat dissipated by Joule effect, Peltier effect...) through the employment of HEATVAL subroutines. The explicit dependence of certain parameters on the temperature can be carried out using FORTRAN written UMAT routines.
- by employing the THERMO ELECTRIC ABAQUS module: This module can be used in the simplest cases (Joule heating only) and for validation.

3.3 Development of a simplified thermoelectric model

The simplified model is also used for identification of the convection coefficient of the composite for numerical simulations of the temperature rise induced by the passage of electrical currents of intermediate intensity.

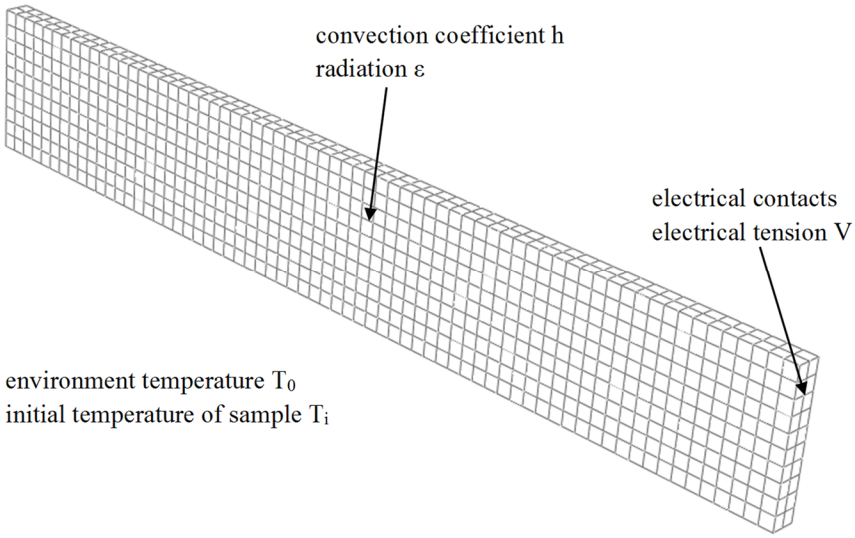

Fig. 3 FEM model with boundary and initial conditions

This simplified thermoelectric models can be developed by neglecting all thermal conduction phenomena: In this case, changes in the conductive medium temperature is governed by the following equation

$$mc_v \frac{dT}{dt} = \boldsymbol{\rho i} \cdot \mathbf{i}V - hA(T(t) - T_a) - \varepsilon\sigma A(T(t)^4 - T_a^4) \tag{34}$$

where m is the mass of the sample and V its volume. At steady state, Eq. 34 takes the following form

$$\boldsymbol{\rho i} \cdot \mathbf{i}V = hA(T - T_a) + \varepsilon\sigma A(T^4 - T_a^4) \tag{35}$$

which expresses the balance between the thermal power dissipated globally (in volume V) and heat exchanged—through the exchange surface S—with the environment by convection and radiation. See also Gigliotti *et al.* 2011 for more details.

3.4 Identification of thermoelectric FE model on experiments on CFRP samples

A 3D FE ABAQUS model has been built and developed based on the equations in sections 3.2 and 3.3, employing the DC3D8E element type, specifically developed for the modeling of the thermoelectric coupling and a total number of 469 elements (see Fig. 3).

The geometric size, the boundary (for an electric current I = 3A) and the initial conditions of atest case example are shown in Table 2 and Table 3. In order to obtain a predefined current value within the sample, a set of electrical tension values are specified at the end surfaces (electrical contacts) of the composite samples (e.g. V_1 = 2.25V and V_2 = 0V for I = 3A), the initial temperature, T_0 (here T_0 = 20°C), is specified in the bulk sample, then convection and radiation boundary conditions are specified on all external surfaces in contact with the environment.

Table 4 shows the all the parameters and properties of the composites samples.

Table 2 Dimensions of the FE model

Length	Width	Thickness
0.165 m	0.018 m	0.002m

Table 3 Boundary and Initial conditions

V_1	V_2	T_0
2.25 V	0 V	20°C

Table 4 Thermoelectric properties for materials CNT/CFRP UD [0]8 used in FE model

Materials	Thermal Conductivity (W/m.K)			Electrical conductivity (S/m)			Specific heat (J/kg.K)
	λ_L	λ_T	λ_E	σ_L	σ_T	σ_E	C_p
Type A	5.73	0.63	0.63	52200	14000	0.51	972
Type B	4.61	0.52	0.52	46600	12000	0.003	874
Radiation exchange	Surface emissive $\varepsilon = 1$					Ambient temperature $T_0 = 20°C$	
Convection exchange	Surface convection coefficient $h = 7$ W/ (m^2. K)					Ambient temperature $T_0 = 20°C$	

Table 5 Thermal properties used for finite element simulations (calibration model) (Toray 2013, Hexcel 2015 Datasheets, Kalogiannakis *et al*. 2004, Villière *et al*. 2013)

	Density	Thermal Conductivity	Specific Heat
	ρ (kg/m3)	λL, λT, (W/m°C)	Cp (J/kg°C)
Fiber T700	1800	λL=9.4, λT=2	753.6
epoxy M21	1280	λL=λT= 0.22	1300

In Table 4, the only "adjusted" coefficient is the convection coefficient, h (h = 7W/m^2K), determined by direct comparison between the experimental and the numerical curve. Electrical conductivities are derived from the electrical measurements illustrated in Fig. 2 the major reservations can be expressed about the validity of σ_T obtained by the law of mixtures (see Eqs. 36-37) (for more detailed discussion, see Lin *et al.* 2015a, b). Thermal properties are calculated from those of the elementary constituents of the composites (T700 fiber and epoxy matrix M21) as taken from the literature (Toray 2013, Hexcel 2015 Datasheets, Kalogiannakis *et al.* 2004, Villière *et al.* 2013, see Table 5) and employing straightforward rule-of-mixtures equations (Eqs. 36-37), with a fiber volume fraction value, V_f, equal to 60%.

For instance, for anisotropic thermal conductivities these equations read

$$\lambda_L = V_f \lambda_f + (1 - V_f)\lambda_m \tag{36}$$

$$\lambda_T = \lambda_m + \frac{\lambda_m(\lambda_R - \lambda_m)V_f}{\lambda_m + \frac{1}{2}(1 - V_f)(\lambda_R - \lambda_m)} \tag{37}$$

where the subscripts f and m indicate, respectively, the fiber and the matrix.

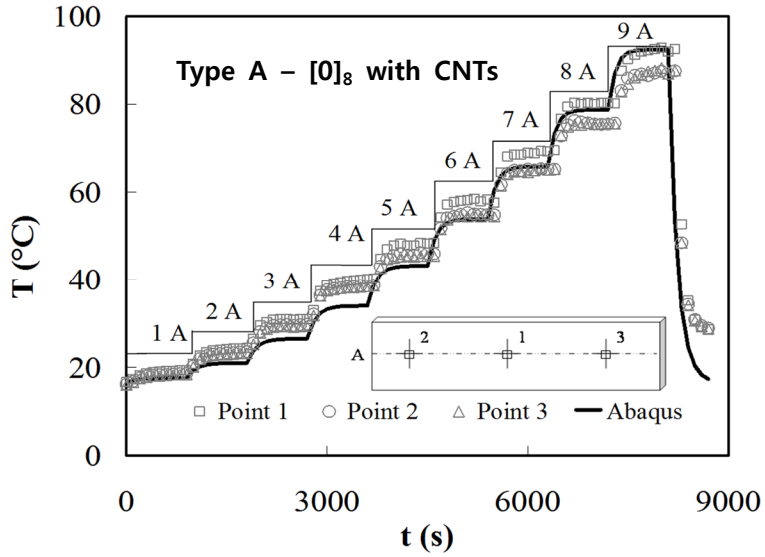

(a) Evolution of the temperature, T (°C), of 3 points located on the sample surface as function of time, t (s)

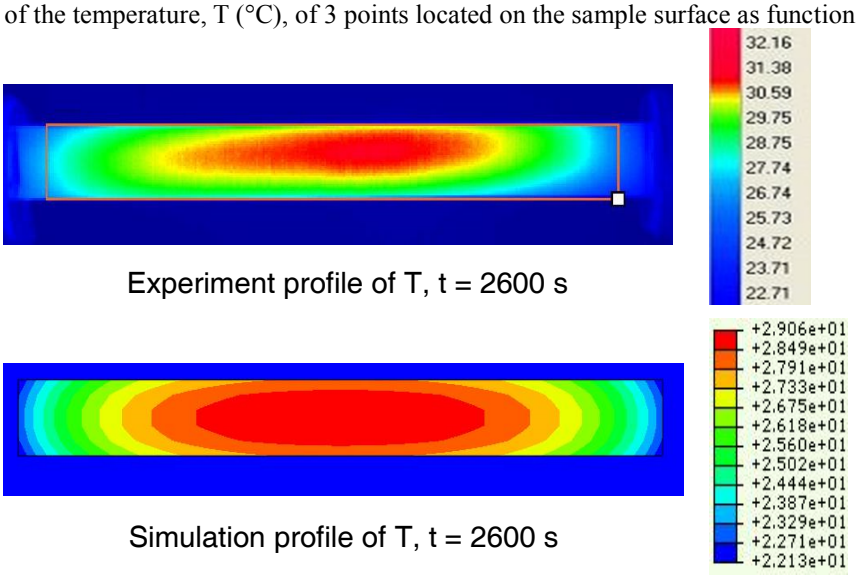

(b) Full temperature fields on the sample surface (t = 2600 s, I = 3A); comparison with ABAQUS numerical simulation for Type A (CFRP/CNT) UDs [0]8 samples

Fig. 4 Simulations results of thermoelectric tests

The thermal properties of CFRP composite samples thus calculated and presented in Table 5 and are in very good agreement with experimental measurements given in Kalogiannakis *et al.* 2004, at room temperature ($C_p \approx 850$ J/ kg°C, $\lambda_L \approx 6$ W/m°C, $\lambda_T \approx 0.6$ W/m°C).

Figs. 4, 5 and 6 illustrate the results of experiments and FE model thermoelectric simulations for CNTs/CFRP (Type A) and CFRP (Type B) composites materials.

Fig. 4a illustrates the evolution of the sample temperature as a function of time, for Type A (CFRP/CNT) UD composite samples, for electric current values from 1A to 9A. Electric current

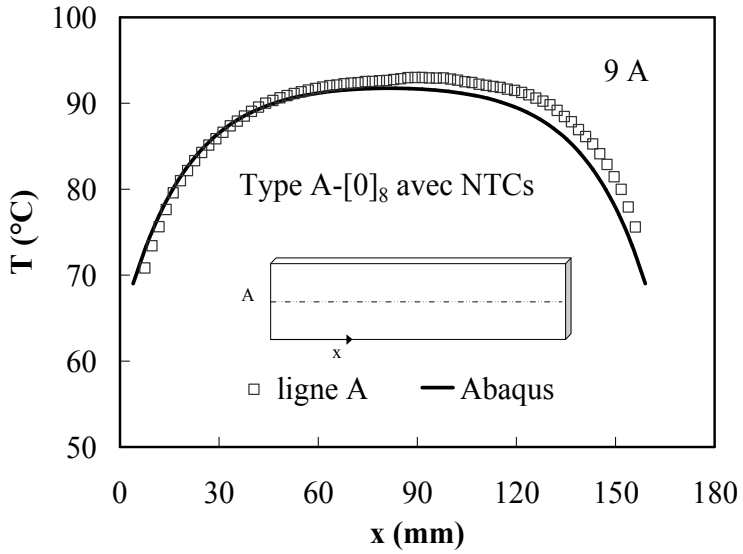

(a) Along the longitudinal centerline (A) for I = 9A (steady-state)

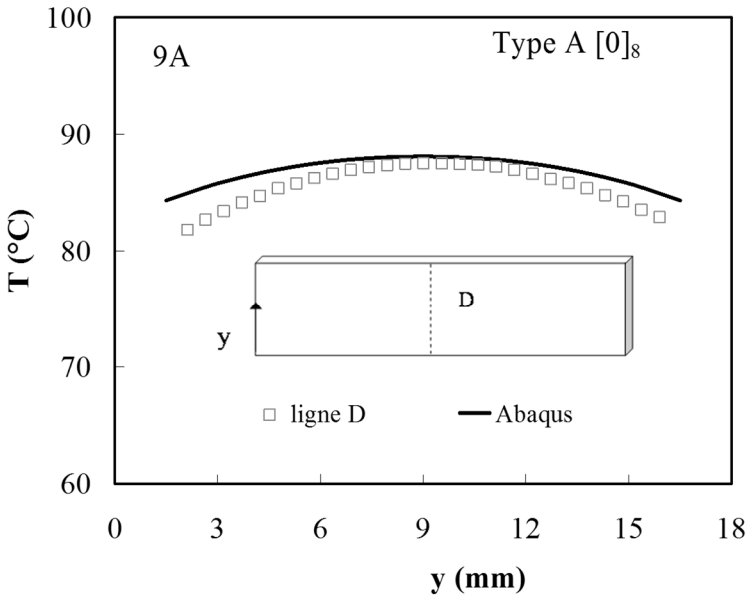

(b) Along the transverse centerline (D) for I = 9A (steady-state)

Fig. 5 Temperature profiles (experimental vs. numerical) on the surface of Type A UD $[0]_8$ sample

are injected in the sample by steps of 1A. The solid curve illustrates the result of the FEM simulation (maximum temperature, calculated at center of the sample external surface), while dotted curve shows the experimental data of three sampling points located at the specimen centerline, along the longitudinal axis: Point 1, located at the sample center, Points 2 and 3, located at a distance of 37.6 mm from Point 1.

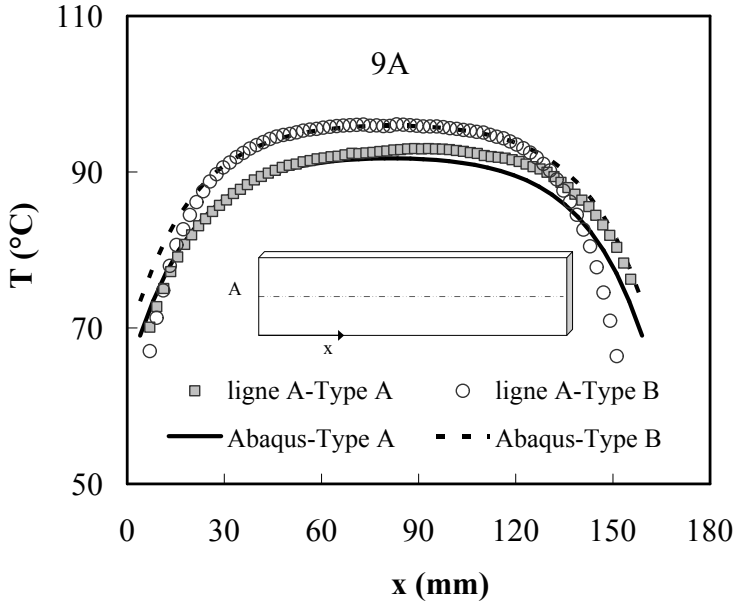

Fig. 6 Profiles of FEM simulations and experimental data: Temperature T versus position x, solid curves show FEM simulation results and dotted curves represent the experimental data, comparisons of Type A et de Type B UD $[0]_8$ (I = 9A).

Fig. 4b illustrates the comparisons between the full experimental temperature field measured by infrared thermography on the external sample surface and the results of ABAQUS numerical simulation, in a transient state, at t = 2600 (I = 3A, maximum measured temperature around 31°C).

Figs. 5a and 5b show, respectively, the temperature profile (experimental vs. ABAQUS numerical simulations) along the longitudinal (A) and transverse (D) centerline of Type A UD $[0]_8$ samples, at I = 9A (steady-state).

Fig. 6 illustrates the temperature profiles (experimental vs. ABAQUS numerical simulations) along the longitudinal (A) centerline of Type A (CFRP/CNT) and Type B (CFRP) UD $[0]_8$ samples, at I = 9A (steady-state). In this case, the additions of CNTs decreases on average the temperature values of around 10%, due to CNT-based electrical conductivity enhanced values for Type A samples.

It is noted that the simulation results are consistent with the experiment data, both in the transient and the steady-state conditions, which validates the pertinence of the thermoelectric FE ABAQUS numerical model over a large range of temperature/electric current values.

4. Numerical simulation of thermoelectric field in composite fuselage-like structures

The ABAQUS FE thermoelectric model developed and identified in previous sections is employed for the simulation of thermoelectric fields generated by the circulation of intermediate electrical current values in composite aeronautical fuselage-like skin structures. These simulations are performed to have orders of magnitude overheating produced by these electrical loads in more or less realistic configurations.

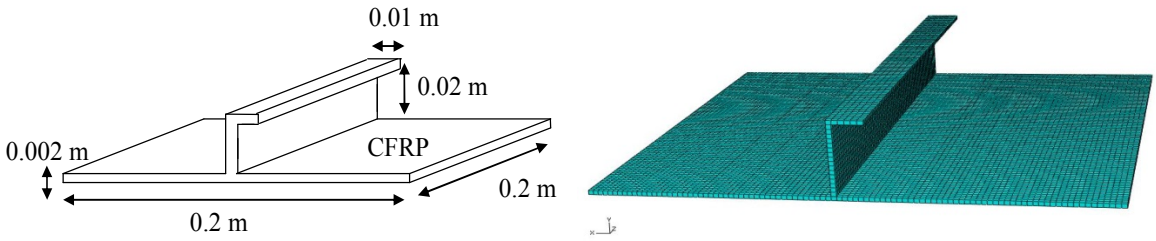

(a) geometry size (b) FE model

Fig. 7 Description and modeling of a structural fuselage-like skin panel piece using the ABAQUS finite element code

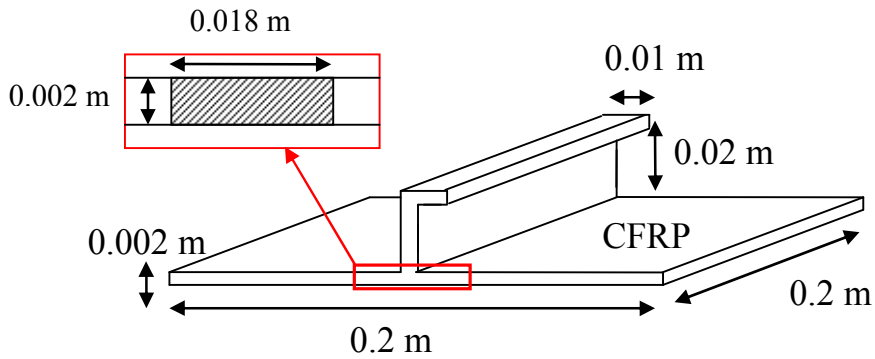

Fig. 8 Schematic of the electric current injection (I = 9A) into the fuselage panel

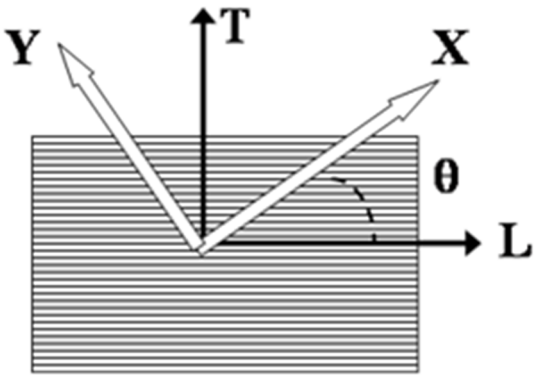

Fig. 9 Schematic defining the angle θ used for the calculation of the electrical and thermal plane anisotropic composite (Eq. 38)

The chosen structural configuration is schematically shown in Fig. 7. For the ABAQUS FE modelling, the DC3D8E element is employed, about 11495 elements.

In this model, an electric current value of 9A is injected through a section of the outer surface of the panel: in Fig 10 the electric current passing section is taken equals to $3.6 \times 10^{-5} m^2$ and the geometry dimension is the same as previous descriptions (same as shown in Fig. 3 and Table 4).

Table 6 Thermoelectric properties of Al material used in the FE model

Density (kg/m^3)	Thermal conductivity (W/mK)	Electrical Conductivity (S/m)	Specific heat (J/kgK)
ρ	λ	σ	C_p
2700	237	3.8×10^7	900

Table 7 Thermal parameters of the FE model

Exchange by radiation	Emissivity $\varepsilon = 1$	Ambient temperature $T_0 = 20°C$
Exchange by convection	Convection coefficient $h = 7$ W/ (m^2. K)	Reference temperature $T_0 = 20°C$

The simulations are performed on $[45/-45/90/0]_s$ quasi-isotropic (QI) stacking sequence structures by using Type A and Type B composite materials: For these configurations, electrical and thermal plane anisotropic properties are calculated starting from the orthotropic values of the elementary ply by using the following relations (for the definition of the angle θ, see Fig. 9)

$$\begin{bmatrix} \sigma_X & \sigma_{XY} \\ \sigma_{XY} & \sigma_Y \end{bmatrix} = \begin{bmatrix} \cos\theta & \sin\theta \\ -\sin\theta & \cos\theta \end{bmatrix} \cdot \begin{bmatrix} \sigma_L & 0 \\ 0 & \sigma_T \end{bmatrix} \cdot \begin{bmatrix} \cos\theta & -\sin\theta \\ \sin\theta & \cos\theta \end{bmatrix} \tag{38}$$

The presented simulations are carried out by employing equivalent homogeneous anisotropic composite elements. The employment of a layerwise model, that is, a model involving an explicit representation of each single ply would possibly lead to better results, both in terms of electrical and thermal transient response. Moreover, this model would allow calculating with accuracy residual stresses at the ply level. The proposed analysis is sufficient to catch the gross thermoelectrical material behavior and for the identification of the main electrical/thermal parameters by inverse analysis of the experimental tests.

A comparison with a panel made of metallic aluminum (Al, corresponding thermoelectric properties given in Table 6) is also performed; the simulations take into account Joule heating due to current flow and heat exchange with the environment (Table 7), associated with convection and thermal radiation, by employing an exchange coefficient by convection h, equals to 7 W/m^2K and an emissivity value near 1. Room temperature is taken equals to 20°C.

Figs. 10-12 illustrate the simulated transient temperature fields ($T - T_0$) at different times in CFRP composite and Al metal materials, subject to the passage of an electric current of intensity equal to 9A.

The figures show that—for the two composite panels—the heating phenomena are located mainly in areas near the surface of the injection current. The anisotropy of the thermoelectric behavior plays a role in the temperature fields which are qualitatively similar for the two considered configurations (Type A and Type B). For the metal panel—because of the high electrical and thermal conductivity—the temperature field is almost homogeneous.

Finally, Fig. 13 compares the time evolution of the maximum temperature rise of the three configurations.

For the three simulated materials, the maximum temperature rise in the panel is reached after about 600s and equal to about 20°C for the metal panel, to about 43°C for the QI CFRP Type A panel and to approximately 49°C for the QI CFRP Type B panel.

(1) Composite panel (IQ-type A) 9A

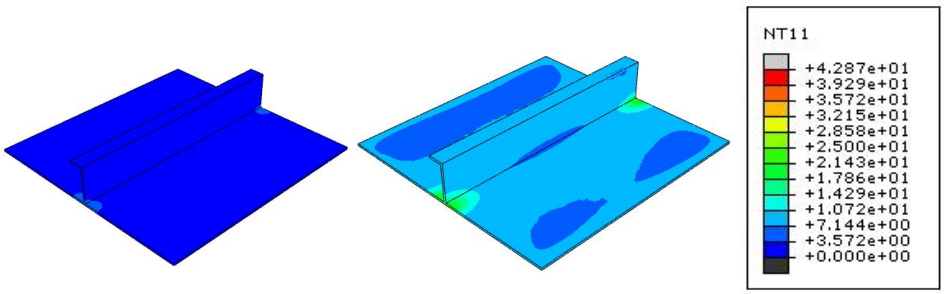

(a) t =10 s (b) t = 60s

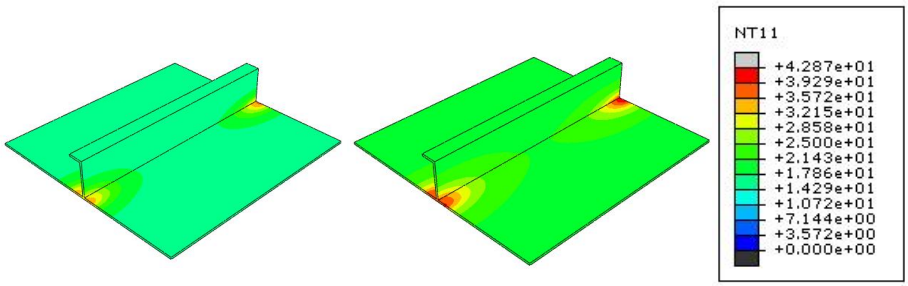

(c) t =200 s (d) t = 500 s

Fig. 10 Transient simulated temperature field in a QI CFRP Type A sample subjected to the transit of an electric current of 9A

(2) Composite panel (IQ-type B) 9 A

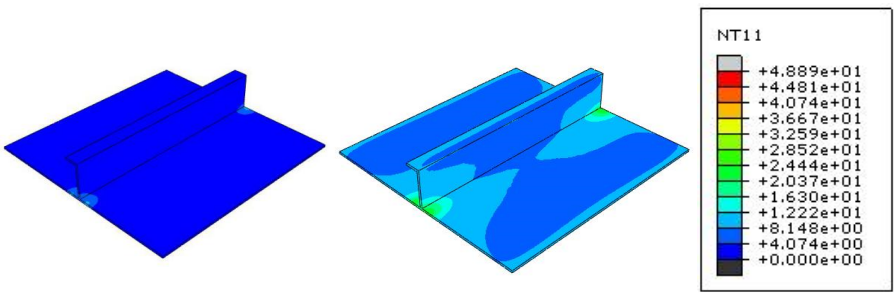

(a) t =10 s (b) t = 60s

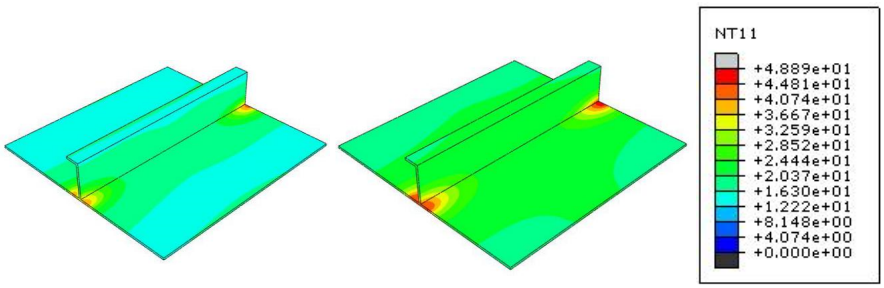

(c) t =200 s (d) t = 500 s

Fig. 11 Transient simulated temperature field in a QI CFRP Type B sample subjected to the transit of an electric current of 9A

(3) Metal panel (Al) 9A

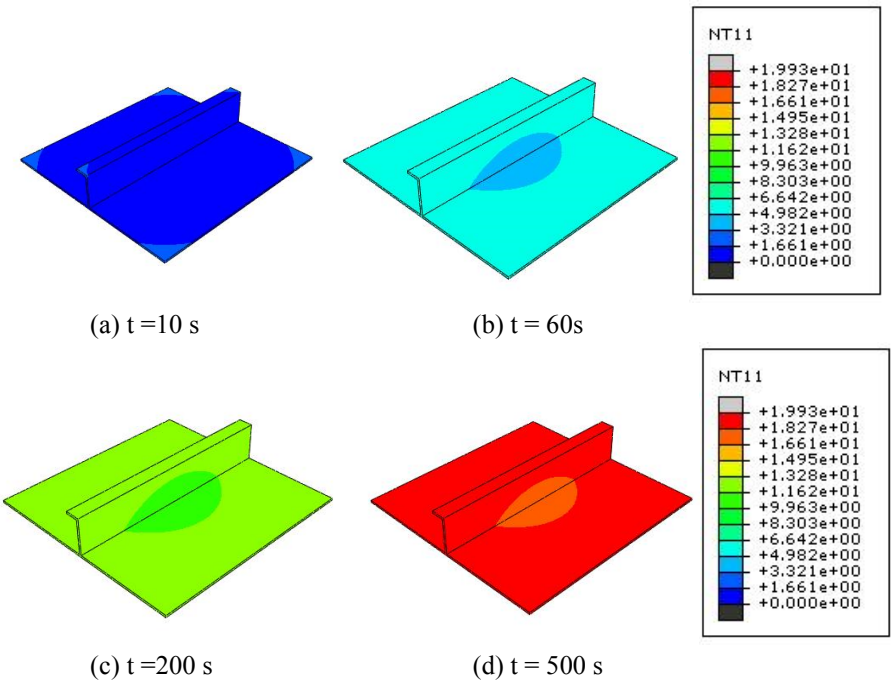

(a) t =10 s (b) t = 60s

(c) t =200 s (d) t = 500 s

Fig. 12 Transient simulated temperature field in Al metal sample subjected to the transit of an electric current of 9A

The presence of the CNTs in Type A CFRP materials helps decreasing by around 7°C the temperature rise with respect to Type B panels, the time needed to reach the maximum temperature value is almost the same for the two composite cases.

5. Conclusions

The paper has presented the development of a model for simulating the thermoelectric behavior of CNTs/CFRP Organic Matrix Composite (OMC) laminates for aeronautical applications. The model has been developed within the framework of the thermodynamics of irreversible processes and implemented into commercial ABAQUS Finite Element software and validated by comparison with experimental thermoelectric tests on two types of composites materials, namely Type A with Carbon Nanotubes (CNT) and Type B without CNT. A simplified model, neglecting heat conduction, is also developed for simplifying the identification process. The model has been then applied for FEM numerical simulation of the thermoelectric response of aircraft panel structures subjected to electrical loads, in order to discuss the potential danger coming from electrical solicitations. The structural simulations have been performed on quasi-isotropic stacking sequences (QI) $[45/-45/90/0]_s$ using composite materials of type A and type B and compared with those obtained on plates made of aluminum metallic material. For both tested cases—passage of electric current of intermediate intensity (9A)—panels made of composite material shows a greater heating than the corresponding metallic ones.

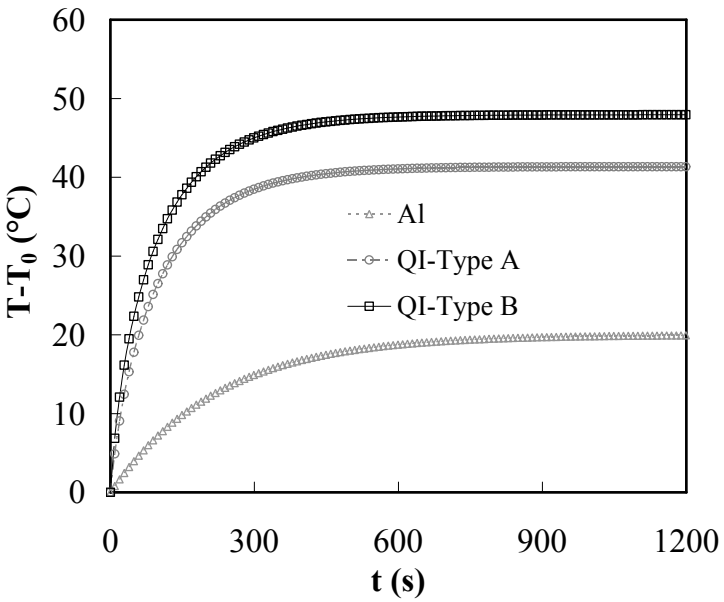

Fig. 13 Simulated evolution of maximum temperature rise over time in QI CFRP Type A, Type B and Al panel subjected to the circulation of electric current of intensity equal to 9A

Perspectives include the employment of refined structural models for a more detailed simulation of the thermoelectrical induced residual strains and stresses at the ply level.

Acknowledgments

The present research was carried out at PPRIME Institute, Department of Physics and Mechanics of Materials, ISAE-ENSMA, Poitiers and in collaboration with ECP MSSMat Lab, Paris. All partners of the research are gratefully acknowledged, some support of CAUC Tianjin is gratefully acknowledged (Project of CAUC: 3122015C010, 2016SYCX04, MHRD20160105).

The research issues touched in the present paper are pertinent with the subjects of the French Government program "Investissements d'Avenir" (LABEX INTERACTIFS, reference ANR-11-LABX-0017-01; EQUIPEX GAP, reference ANR-11-EQPX-0018).

References

Dassault Systemes Simulia Corp. (2009), *ABAQUS Ver. 6.9.*, Providence, RI, U.S.A.

De Groot, S.R. and Mazur, P. (1969), *Non-equilibrium thermodynamics*, North Holland Publishing Company, Amsterdam, The Netherlands.

Gigliotti, M., Lafarie, M.C. and Grandidier, J.C. (2011), "Development of experimental and modeling tools for the characterization of the thermo-electro-mechanical behavior of composite materials for aircraft applications", *Mech. Industry*, **12**(2), 87-101.

Gigliotti, M., Lafarie-Frenot, M.C., Lin, Y. and Pugliese, A. (2015), "Electro-mechanical fatigue of CFRP laminates for aircraft applications", *Compos. Struct.*, **127**, 436-449.

Hexcel Corporation (2015), 180°C curing epoxy matrix; Hexcel Corporation, CT, U.S.A. https://www.hexcel.com/user_area/content_media/raw/HexPly_M21_global_DataSheet.pdf

Kalogiannakis, G., Hemelrijck, D. and Assche, G. (2004), "Measurements of thermal properties of carbon/epoxy and glass/epoxy using modulated temperature differential scanning calorimetry", *J. Compos. Mater.*, **38**(2), 163-175.

Lin, Y., Gigliotti, M., Lafarie-Frenot, M.C. and Bai, J. (2015a), "Experimental study to assess the effect of carbon nanotube addition on the through-thickness electrical conductivity of CFRP laminates for aircraft applications", *Compos. Part B Eng.*, **76**, 31-37.

Lin, Y., Gigliotti, M., Lafarie-Frenot, M.C. and Bai, J. (2015b), "Effect of carbon nanotubes on the thermoelectric properties of CFRP laminate for aircraft applications", *J. Reinf. Plast. Comp.*, **34**(2), 173-184.

Muller, I. (1973), *Thermodynamik*, Bertelsmann, Dusseldorf, Germany.

Saba, J., Magga, Y., He, D., Miomandre, F. and Bai, J. (2013), "Continuous electrodeposition of polypyrrole on carbon nanotube-carbon fiber hybrids as a protective treatment against nanotube dispersion", *Carbon*, **51**, 20-26.

Schulte, K. and Wittich, H. (1995), "The electrical response of strained and or damaged polymer-matrix composites", *Proceedings of ICCM10 Canada*, British Columbia, Canada, August.

Sierakowski, R.L., Telitchev, I.Y. and Zhupanska, O.I. (2008), "On the impact response of electrified carbon fiber polymer matrix composites: Effects of electric current intensity and duration", *Comp. Sci. Tech.*, **68**(3-4), 639-649.

Toray Carbon Fibers America, Inc. (2013), Title of website link; Toray Industries, AL, U.S.A. http://www.toraycfa.com/pdfs/T700SDataSheet.pdf.

Villière, M., Lecointe, D., Sobotka, V., Boyard, N. and Delaunay, D. (2013), "Experimental determination and modeling of thermal conductivity tensor of carbon/epoxy composite", *Compos. Part A Appl. Sci. Manuf.*, **46**, 60-68.

Xia, Z.H., Okabe, T., Park, J.B., Curtin, W.A. and Takeda, N. (2003), "Quantitative damage detection in CFRP composites: Coupled mechanical and electrical models", *Comp. Sci. Tech.*, **63**(10), 1411-1422.

Zhao, Z.G., Ci, L.J., Cheng, H.M. and Bai, J.B. (2004), "Growth of multi-walled carbon nanotube of different morphologies on carbon fibres by floating catalyst method", *Carbon*, **43**, 663-665.

EC